Experiment on Fatigue Performance of Joints of Upper Plate and U-shape Stiffening Rib at Diaphragm

YU Tian-hao[1], JIANG Yin-long[2]

1. College of Civil Engineering, Tianjin University, Tianjin 300072, China;
2. College of Civil Engineering, Tongji University, Shanghai 200092, China

Abstract
Owing to its high strength and stiffness, the orthotropic steel deck system has been widely used in the construction of long-span steel bridges. For many detailed parts of the orthotropic steel deck system, the fatigue strength curves have been given. However, studies on the fatigue performance of joints of upper plate and U-shape stiffening rib at diaphragm are limited, especially for joints made with the wielding process in China. In this paper, experiment study on fatigue performance of joint of upper plate and U-shape stiffening rib at diaphragm of orthotropic bridge deck in Hangzhou Zhijiang Bridge was conducted. With this experiment, the distribution and variation of stress of the joint under fatigue loads were revealed, and the fatigue strength of the joint was tested. In addition, finite element model of the specimen and the test equipment was established for analysis. The results of the experiment show that fatigue cracks are not found with naked eyes, after a total of 2.9 million times of cyclic loading, during which the minimum load range is 10t and the maximum load range is 35t. This means the fatigue performance of the joint is good. The test results and finite element analysis results are in good accordance, which achieved a mutual verification and proves the reliability of the experiment.
Keywords: FATIGUE PERFORMANCE, UPPER PLATE, U-SHAPE STIFFENING RIB, EXPERIMENT STUDY, FINITE ELEMENT ANALYSIS

Introduction

The orthotropic steel bridge deck system is composed of bridge decks, diaphragms, and longitudinal and transverse stiffening ribs. Owing to its light weight, high strength and other characteristics, it is now the major bridge deck form of long-span steel bridges[1-3]. And since closed section U-shape rib stiffened plates have better rigidity compared with open section ones, the U-shape stiffening rib has become a common part of orthotropic bridge deck[4]. Scholars have done lots of experiments to gain a better understanding of the structural details of orthotropic steel deck, and for most of the details, S-N curves (fatigue strength curves) have been given in the structural design codes or specifications. But so far, few studies have been conducted on the fatigue performance of joints of upper plate and U-shape stiffening rib at diaphragm. Although scholars in Japan and Netherlands conducted some fatigue tests on this detail by means of small specimen[5-6], the gaps between domestic and foreign welding process prevent scholars in

China from relying on the results of foreign researches, because the fatigue performance of the detail is in close relationship with the well-being of processing-like the welding process. Thus, it is necessary to carry out more studies on the fatigue behavior of joints of upper plate and U-shape stiffening rib at diaphragm.

In this study, a full-scale model of orthotropic bridge deck was made to study the fatigue performance of the joint. The purpose of this fatigue test is to provide the basis for the selection of fatigue

curves during the steel bridge design, to accumulate data for deciding the S-N curve of structural details in Chinese steel bridge design code, and to verify the fatigue strength of the structural detail of the steel bridge deck in Hangzhou Zhijiang Bridge.

1. The Design and Test of the Specimen

1.1. The Design and Manufacture of the Specimen

The specimen for the fatigue test was designed according to the orthotropic bridge deck in Hangzhou Zhijiang Bridge, for the purpose of reflecting the stress characteristics and structural details of the joint of the real bridge. The specimen and test devices are shown in Figure 1. The major parts of the specimen are the upper plate, the three U-shape stiffening ribs in the horizontal direction along the bridge, and a diaphragm at mid-span. The webs on the left and right sides of specimen were set to simulate the constraining effect of nearby plates on the specimen. The base was set at the bottom of the diaphragm to increase the bending stiffness of the specimen, and to make it easier to fix the specimen on the reaction frame. More importantly, the arrangement of the webs and the base can make the stress distribution of the specimen much more similar to that in the real bridge. The total width of the specimen is 1860mm, and the total longitudinal length of it, which is the length along the bridge, is 400mm. Under the real circumstances, the distances between the diaphragms and the thicknesses of the diaphragms are inconstant. However, given the limitation of resources available, it is impossible to test them all. So here, only the most unfavorable condition is considered, and the thickness of the diaphragm is set as 10mm, which is the minimum value of the thickness of the diaphragms in the real bridge. Other thicknesses of the specimen are the same as the real bridge. To reflect honestly the fatigue performance of the actual bridge, the welding process of welds between the diaphragm and the upper plate, the diaphragm and the U-shape stiffening rib, and the upper plate and the U-shape stiffening rib are the exactly the same as those of the real bridge.

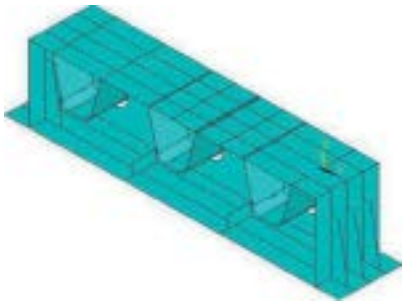

(a) Three-dimension schematic diagram of the specimen

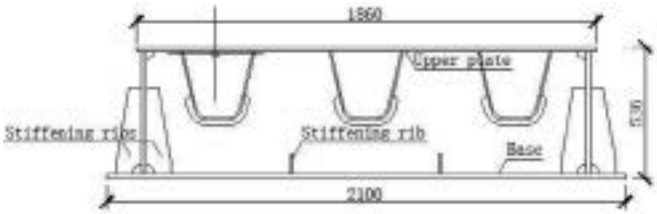

(b) Front view of the specimen

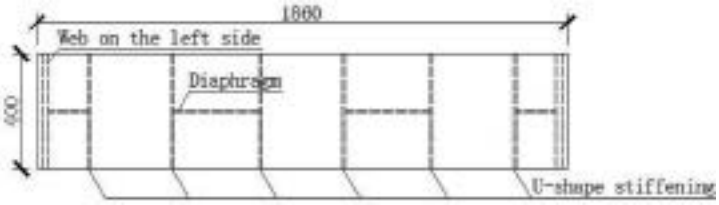

(c) Top view of the specimen

Figure 1. Schematic diagram of the specimen (Unit: mm)

1.2. The Test Devices and Loading Schemes

In general, the loading system of this fatigue test is composed of three parts: the mechanical system, the hydraulic system, and the electric control system. The jack is used to load, and an elastic support is set between the jack and specimen for the simulation of the wheel pressure. Single-axle and two-wheel load was applied to the specimen. The nomenclature 'single-axle and two wheel load' means there is one axle, and there are two wheels on both sides of the axle, which are four wheels in total. However, when the width of the specimen and the length of the axle are considered, it is easy to see that there is enough space for only the two wheels on one side of the axle to be placed on the specimen. The place where the load of the two wheels is applied to the specimen and the width of the two wheels are shown in Figure 3a. In order to save time, two specimens were placed on the reaction frame at the same time, so that two specimens can be tested simultaneously. The layout of the experiment is shown in Figure 2.

In the early stage of the test, the maximum load value was controlled to be around 11t, and the minimum load value was controlled to be around 1t. Thus,

(a) The actual layout of the experiment

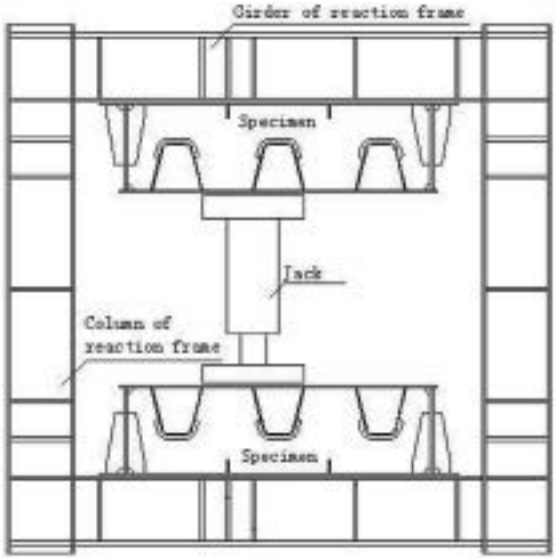

(b) The schematic diagram of the layout of the experiment

Figure 2. The layout of the experiment

the load range was about 10t. After two million times of cyclic loadings, during which the load range was 10t, the load range was increased by 5t at each following load steps. The number of cyclic loadings at each step was determined according to the real circumstances. Finally, the loading process was stopped when the number of loading cycles reached 2.9 million. Throughout the entire time, the minimum load value is around 1t, and the changes in the load range are achieved by the increases of the maximum load value.

1.3. Test Content and Layout of Stain Gages

Tests of the strains primarily focused on the upper plate, the web of U-shape stiffening rib, and part of the diaphragm that is near the welding hole[10-12]. The types of strain gages utilized are tee strain gage rosette and rectangular strain gage rosette. The numbering rules of channels(strain gages) are as follows:

(1) The letter 'D' represents the dynamic signal acquisition channel. The letter 'J' represents the static signal acquisition channel.

(2) The hundreds digit indicates which plate the strain gage is located, that is, '1' represents that the strain gage(channel) is on the upper plate,'2' represents that the strain gage is on the diaphragm near the welding hole, and '3' represents that the strain gage is on the web of the U-shape stiffening rib.

(3) The tens digit indicates the direction of strain gages, that is, '1' means the direction along the bridge, '2' means the direction transverse to the bridge, '3' means the vertical direction, and '4'means the direction of the strain gage in a rectangular strain gage rosette that has a 45 degree angle with both of the other two strain gages.

(4) The units digit is introduced to distinguish the numbers of the channels that are of the same type, on the same plate, and measuring strains in the same direction.

For example, 'D111' means the first dynamic signal acquisition channel which is on the upper plate and placed in the direction that is along the bridge.

The arrangement of strain gages on a single specimen is as follows:

The strain gage rosettes of the upper plate are arranged on the bottom of the plate near the three-direction cross-weld. Tee strain gage rosettes are applied there. There are three strain gage rosettes on either side of the diaphragm, that is, six rosettes in all, including four dynamic and two static signal acquisition rosettes. Each strain gage rosette has two channels(gages), in which one is along the bridge, and the other is in the transverse direction of the bridge. Thus, in total, there are twelve channels on the upper plate, including eight dynamic and four static signal acquisition channels. The tee strain gage rosettes on the upper plate are shown in Figure 3a.

The strain gage rosettes on the diaphragm near welding holes are rectangular strain gage rosettes, and they are placed where the curvature of the edges of the holes change greatly. Six rosettes are arranged on one single side of the diaphragm, including four dynamic and two static signal acquisition rosettes. Each rosette has three channels(gages), which are channels for the direction along the bridge, the direction transverse to the bridge, and the direction of the gage in a rectangular rosette that has a 45 degree angle with both of the other two strain gages. In sum, there are eighteen channels on the diaphragm near the welding holes, including twelve dynamic and six static signal acquisition channels. The rectangular strain gage rosettes on the diaphragm are shown in Figure 3b.

The strain gage rosettes on the webs of U-shape stiffening ribs are tee strain gage rosettes, and they are located at places on the ribs that are close to the

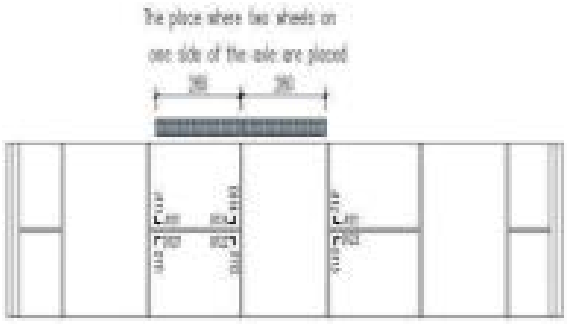

(a) Arrangement of strain gage rosettes on the upper plate

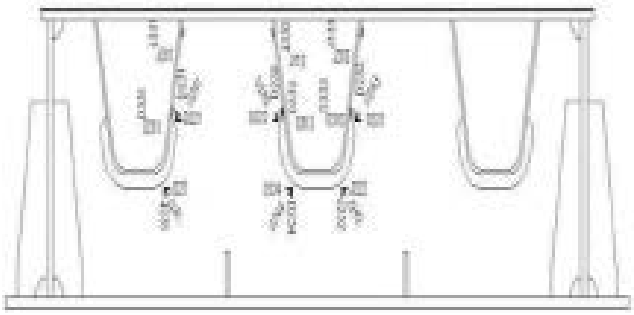

(b) Arrangement of strain gage rosettes on the diaphragm and the web of U-shape stiffening rib

Figure 3. Arrangement of strain gage rosettes (Unit: mm)

welding connection between the web of U-shape stiffening rib and the diaphragm. Six strain gage rosettes are placed on the webs of U-shape stiffening ribs, including three dynamic and three static signal acquisition rosettes. Each rosette has two channels(gages), which are channels for the direction along the bridge and the vertical direction. In total, there are twelve channels on the U-shape stiffening ribs, including six dynamic and six static signal acquisition channels. The tee strain gage rosettes just mentioned are also shown in Figure 3b.

2. Test Results

During the loading process, strains were only recorded when the variation law of the load is relatively stable. Take the channels of upper plate, which are channel D122, D123 and D124, for example. The strains collected from these three channels in one second are shown in Figure 4a. The time history of the strains are sinusoidal curves, whose periods and variation laws match well with the time history of the load that is shown in Figure 4b.

As can be seen from Figure 4, the maximum and minimum load values of different cycles are not the same, thus, the load ranges of different loading cycles are different. Due to the huge number of loading cycles, a thorough collection of load ranges will consume a lot of time and manpower. Therefore, a simple method is applied here to facilitate the recording of data. The first step of the method is to select a series of continuous data(maximum and minimum load values of several nearby loading cycles) as samples during the time when the variation law of the time history of the load is stable. Then compute the load ranges by using the data gained in the step above. After that, calculate the arithmetic mean of the above mentioned load ranges as the load range within this period of time during which the data in first step are collected. At the same time, count and make a record of the number of loading cycles corresponding to this arithmetic mean. Up till this step, different load ranges in one given period of time are represented by the arithmetic mean of these load ranges reappearing in this period of time for a counted number of times. Moreover, for loading processes in different time periods, we can apply this method again when the arithmetic means of load ranges in diverse time periods are similar to each other. That is, calculate a new arithmetic mean out of the average load ranges(the old arithmetic means in one period), which is the arithmetic mean of several time periods. After that, count the total number of cyclic loadings involved in all the time periods that are related to the new arithmetic mean. This new arithmetic mean of load ranges reappear-

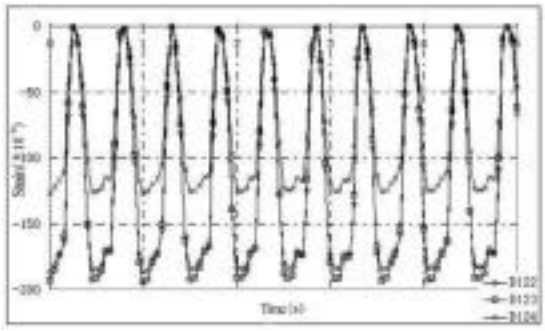

(a) Time history of the strains

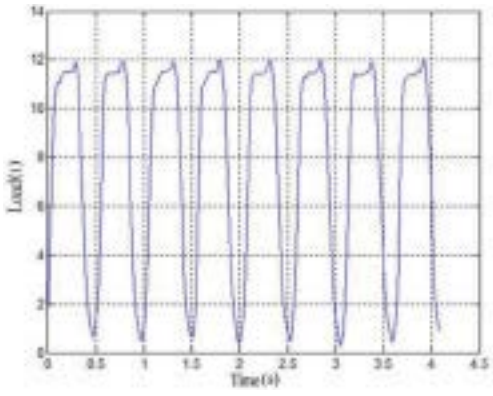

(b) Time history of the load

Figure 4. Time history of the strains and the load

ing during the several periods of time for a counted number of times could be used to represent all the load ranges in these time periods. With this method, the load ranges during several periods of time can be recorded with and represented by a reduced number of data. This method can not only save the time and manpower, but also reflect the actual load ranges to a certain acceptable degree.

The steps of this method are listed as follows:

(1) The load range $F_{i,j}$ is calculated by using the maximum and minimum load values($F_{i,j\max}$ and $F_{i,j\min}$) collected, as is shown in equation(1).

(2) Count the number of loading cycles in time period i. The sum of $n_{i,j}$, which is n_i, is the total number of loading cycles in period i. Then calculate the arithmetic mean of all load ranges in time period i according to equation (2). The result F_i is the representing load range in period i.

(3) For different time periods(like the above mentioned time period i), take average load ranges of several individual time periods(like $\overline{F_i}$) as samples and repeat the steps above again, when the representing average load ranges of the periods considered are similar. Then, count the number of loading cycles in all the time periods involved, which is the sum of n_i. Finally, calculate the arithmetic average of $\overline{F_i}$ according to equation(4). The result $\overline{F}$ is the representing load range of the several nearby periods of time considered.

$$F_{i,j} = F_{i,j\max} - F_{i,j\min} \quad (1)$$

$$\overline{F_i} = \frac{\sum\left(n_{i,j}F_{i,j}\right)}{n_i} \quad (2)$$

$$n_i = \sum n_{i,j} \quad (3)$$

$$\overline{F} = \frac{\sum\left(n_i\overline{F_i}\right)}{\sum n_i} \quad (4)$$

The examples of the process of calculations and related results are shown in Table1-3.

3. Comparative Analysis of Experimental and Finite Element Results

In order to verify the reliability of the results from the fatigue test, the finite element model of both the specimen and the reaction frame is created with the help of the finite element software ANSYS, and the strains measured from the fatigue test is compared with the corresponding theoretical strains of the finite element model[13-16]. The finite element model is shown in Figure 5. Because of the large stiffness of the reaction frame, its deformation is extremely small during the process of loading. So it is enough to ap-

Table 1. Load ranges calculated via maximum and minimum load values collected (Unit: t)

Number of the period	Period 1	Period 2	Period 3
$F_{i,j}$ (Load range calculated directly from data collected)	10.29	10.95	11.19
	10.74	10.54	11.13
	10.45	10.77	10.71
	10.56	10.37	10.90
	10.72	10.81	10.86
	10.22	10.49	10.94
	10.58	10.44	11.04
	10.76	10.96	10.87
$\overline{F_i}$ (Arithmetic mean of load ranges in one period)	10.54	10.67	10.96

Number of the period	Period 4	Period 5	Period 6
$F_{i,j}$ (Load range calculated directly from data collected)	10.37	10.66	10.79
	10.33	11.34	10.60
	10.39	11.11	10.81
	10.49	10.47	10.60
	10.80	11.23	10.81
	10.81	10.94	10.60
	10.70	11.00	10.56
	10.75	10.94	10.86
$\overline{F_i}$ (Arithmetic mean of load ranges in one period)	10.58	10.96	10.70

Table 2. Final average load range of different time periods (Unit: t)

$\overline{F_i}$ (Arithmetic mean of load ranges in one period)	10.54	10.67	10.96
n_i (Number of loading cycles of each $\overline{F_i}$)	40,400	48,035	52,374
$\overline{F_i}n_i$	425,816	512,533	574,019
$\sum n_i$	283,724	$\sum\left(\overline{F_i}n_i\right)$	3,049,665

$\overline{F_i}$ (Arithmetic mean of load ranges in one period)	10.58	10.96	10.70
n_i (Number of loading cycles of each $\overline{F_i}$)	43,658	51,325	47,932
$\overline{F_i}n_i$	461,902	562,522	512,872
$\sum n_i$	$\overline{F}$	10.75	

Table 3. Summary of load ranges and number of cyclic loadings of each load range throughout the entire experiment (Unit: t)

Average load range of several periods	Corresponding number of loading cycles
9.5	154,267
10.5	963,090
11.0	1,046,014
11.5	23,977
13.0	78,661
13.5	22,211
14.0	36,826
20.5	129,789
26.0	108,168
30.2	92,071
33.5	251,055

ply fixed constraint only at the bottom of the reaction frame. Contact elements are established to simulate the interaction between the specimen and the reaction frame. That is, transfer the force and displacement between the two parts. The load range of the load of the finite element model is set as 10t. Finally, the strains of the finite element model that are corresponding to the strains measured by the strain gage rosettes in the fatigue test are collected after computation, and the time history curves of the strains from finite element analysis can be fitted. The period of the time history of the strains should be in accordance with the period of the loading cycle.

The data from channel D122, D124, and D123, which are located on the upper plate(shown as Figure 3), and the data from channel D233, and D232, which are located on the diaphragm near the welding hole(shown as Figure 3) are selected in this comparative analysis. Among them, channel D122, D124, and D123 measure strains in the transverse direction of the specimen, and the channel D232 and D233 measure vertical strains of the diaphragm near the welding hole, especially the strains of the diaphragm that are near the small arc. Since the load ranges of the loading cycles at the time the strains were collected are different, it is hard to compare the strains. Thus, corrections have to be made. In this study, the strain collected when the load range is 10t is set as the standard, and the strain collected not under such a condition should be multiplied by a correction coefficient, which equals to10t divided by the load range related to the strain. This correction is based on the linear elastic assumption, which here means that the relationship between the load range and the strain is linear. For selected channels, Figure 6a-e show the comparisons of actual strains from the test and theoretical strains from finite element analysis when the

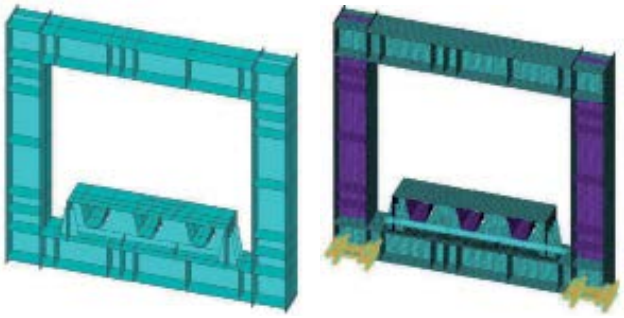

Figure 5. Finite element model of the specimen and the reaction frame

specimen or model was subjected to different numbers of loading cycles.

Figure 6a shows that the measured strains and theoretical strains collected from are in certain accordance, except for the results of 2.75 million times of cyclic loading. The reason why the accordance is not perfect could be that friction exists between individual part of the force transferring devices, including the girder used to distribute the load and the arc-shape backing plate. And the friction will reduce the force that is ultimately transmitted to the specimen. As a result, the measured strains of the fatigue test are smaller than theoretical values of strains gained from the finite element analysis. This phenomenon, which indicates that the test results are smaller than the theoretical values, could also be seen through the results of channel D123 and channel D124, as is shown in Figure 6b and Figure 6c. As for the results of 2.75 million times of cyclic loading, the corrected strains of the test are much smaller than both the strains of other times of cyclic loading and the theoretical value. That is, when the load range increased from 10t at the beginning of the test to 30t when the strains were collected, which is 2 times larger than 10t, the strain only increased 1.4 times. Thus, when corrected by the coefficient, the strains are much smaller. This means that when the absolute value of the load is too large, the proportion of load transmitted to the specimen has been reduced severely. There could be two possible reasons leading to this fact: one is that the accuracy of oil pressure sensor reduces when the oil pressure is too high, the other is the large friction between the cylinder piston rod and the cylinder wall.

The phenomenon that can be seen from Figure 6b is similar to that of Figure 6a except that results in Figure 6b disperse a little bit more widely. This may be because channel D123 is located at the edge of the loading zone, and could be affected greatly by the unevenness local loading. As is shown in Figure 6c, several curves of the measured strain deviates from the theoretical strain curve. To have a better understand-

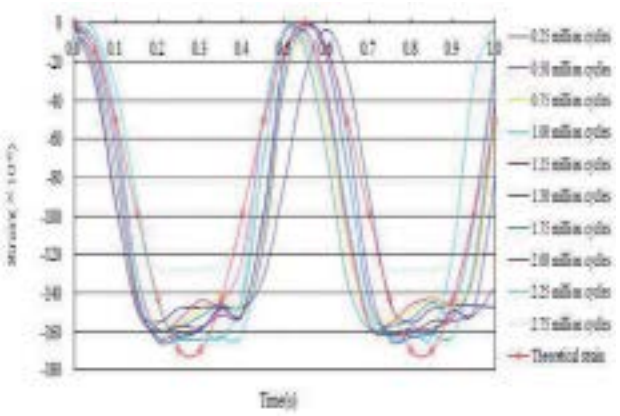

(a) Comparison between the time histories of experimental strains and theoretical strains of channel D122

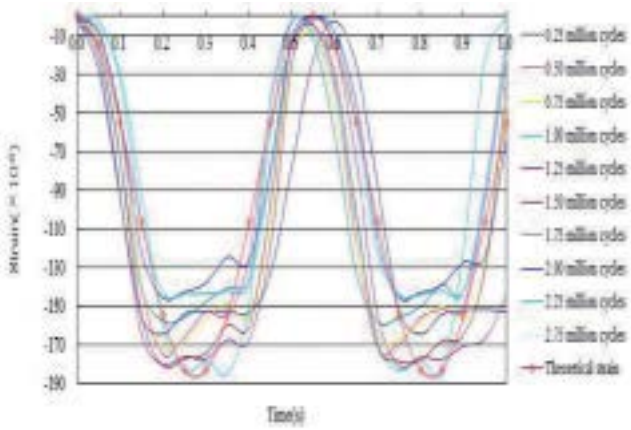

(b) Comparison between the time histories of experimental strains and theoretical strains of channel D123

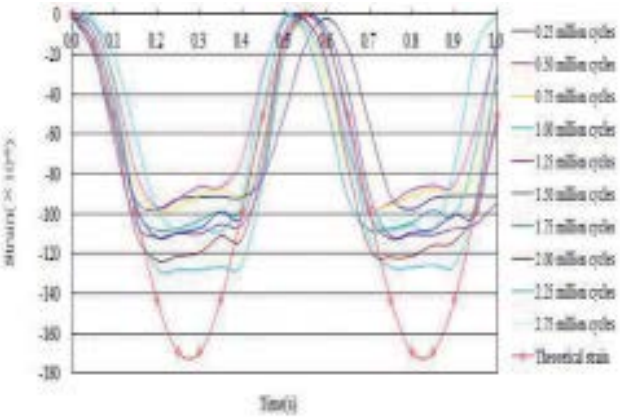

(c) Comparison between the time histories of experimental strains and theoretical strains of channel D124

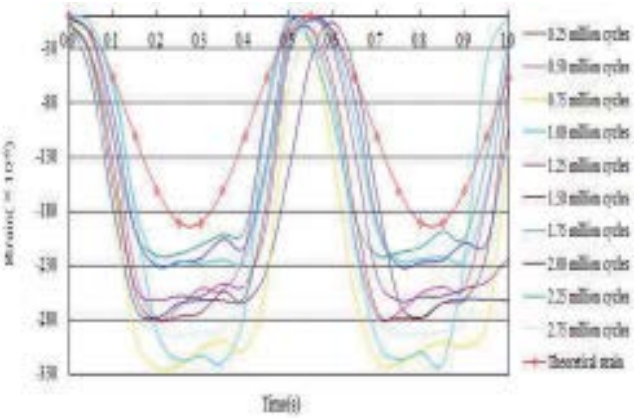

(d) Comparison between the time histories of experimental strains and theoretical strains of channel D232

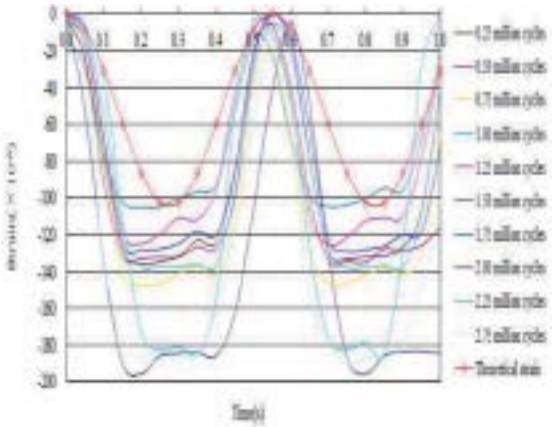

(e) Comparison between the time histories of experimental strains and theoretical strains of channel D233

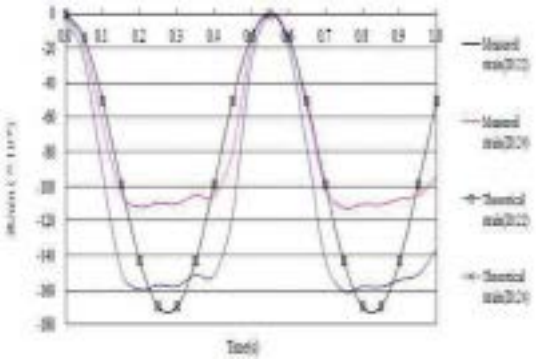

(f) Comparison between the time histories of channel D122 and channel D124

Figure 6. Comparisons between theoretical strains and experimental strains

ing of this issue, an addition comparison of channel D122 and D124-the two channels symmetrically distributed on both sides of the diaphragm-is made, as is shown in Figure 6f. The theoretical strains of channel D124 and channel D122 in Figure 6f are strains after 1.25 million times of cyclic loading. As can be found in Figure 6f, the theoretical strain curve of channel D122 is consistent with that of channel D122, while the measured strains from channel D122 and D124 do not match well. The reason for this could be as follows. The main deformation of the specimen in the finite element model is bending, and there is almost no torsion, which is the theoretical condition. While during the test, the specimen has a certain degree of torsional deformation due to the asymmetric load transmission. This torsion of the specimen should be

responsible for the differences between the measured strains of channel D122 and channel D124.

Large deviations exist between the measured and theoretical strain curves of different number of cyclic loadings in both Figure 6d and 6e. Moreover, the individual measured strain curve of one channel is not consistent with each other. These might due to the unevenness of load transmission and the out-of-plane bending deformation of diaphragm, which is caused by the torsion of the specimen. In addition, during the test, the specimen once appeared to move to the column of reaction frame, resulting in the extrusion of reaction frame. And this interaction between the specimen and the reaction frame, which is caused by the movement of the specimen, could affect the stress state and deformation characteristics of the diaphragm.

Since the fatigue test in this paper focus mainly on the connection of the upper plate and the U-rib, and the measured strains of channel D122 and D123, which are channels related to the connection, are in good agreement with the theoretical values of the strains, especially when the number of loading cycles is within 2.5 million at the start of test, it is reasonable to come to the say that the results of the fatigue test are trustworthy, although there are some deviations between the measured and theoretical strains in the final stage of the test.

Conclusions

Through the observation of the experimental phenomenon, and the analysis of the experimental results and finite element results, the following conclusions are come to:

(1) In this study, the Hangzhou Zhijiang Bridge was taken as the engineering background, the joint of upper plate and U-rib at diaphragm was selected as the research object, and a full-scale model was designed to conduct the fatigue test. The total number of loading cycles was 2.9 million. The minimum load range was 10t, and the maximum range was 35t. After cyclic loadings, fatigue cracks were not found with naked eyes, which means the fatigue performance of the joint is good.

(2) The fatigue test in this study focused mainly on the connection between upper plate and U-rib. So the channels related to this connection, which are channel D122 and D123, are the major concerns. The measured strains of channel D122 and D123 are in good agreement with the theoretical values-the results of the finite element analysis-within 2.5 million loading cycles at the start of the test. Thus, even though there are some inconsistencies between the measured strains and the theoretical values in the later stage of the experiment, the test results are reliable in general, and can be used to determine the fatigue strength curve of the detail studied.

References

1. Huang Wei. Theory and method of long-span steel bridges deck pavement design. China Architecture & Building Press, 2006,pp.331-335.
2. Kim T W, Baek J, Lee H J, et al. Effect of pavement design parameters on the behavior of orthotropic steel bridge deck pavements under traffic loading. International Journal of Pavement Engineering, 2014, 15,pp.471-482.
3. Chen S J, Yang K C. Inelastic behavior of orthotropic steel deck stiffened by U-shaped stiffeners. Thin-Walled Structures, 2002, 40,pp.537-553.
4. De Freitas S T, Kolstein H, Bijlaard F. Composite bonded systems for renovations of orthotropic steel bridge decks. Composite Structures, 2010, 92,pp.853-862.
5. Yasuda O, Takaba S, Morishita Y, et al. Study on improvement of fatigue strength for steel plate deck bridge by using fatigue proof steel. Composite Structures,2007, 10,pp.46-49.
6. Bakker M C M, De Jong F B P. Ultrasonic underside inspection for fatigue cracks in the deck plate of a steel orthtropic bridge deck. HERON, 2003, 48,pp.277-295.
7. WAN Peng, ZHENG Kai-feng. Fatigue performance of orthotropic deck of railroad bridges. World Bridges, 2004, 11,pp.44-48.
8. Jeong Y S, Kainuma S, Ahn J H. Structural response of orthotropic bridge deck depending on the corroded deck surface. Construction and Building Materials, 2013, 43,pp. 87-97.
9. Yao B, Cheng G, Wang X, et al. Characterization of the stiffness of asphalt surfacing materials on orthotropic steel bridge decks using dynamic modulus test and flexural beam test. Construction and Building Materials, 2013, 44,pp. 200-206.
10. YANG Yong, ZENG Su-sheng, XUE Jian-yang, et al. Fatigue performance test of steel plate-concrete hollow composite deck. China Journal of Highway and Transport, 2011, 24,pp. 44-50.
11. Cho K, Cho J R, Chin W J, et al. Bond-slip model for coarse sand coated interface between FRP and concrete from optimization technique. Computers and Structures, 2005, 84,pp. 439-449.

12. King L, Toutanji H, Rajesh Vuddandam. Load and resistance factor design of fiber reinforced polymer composite bridge deck. Composites Part B: engineering, 2012, 43,pp.673-680.
13. Davey S W, Van Erp G M, Marsh R. Fibre composite bridge decks—an alternative approach. Composites Part A: Applied Science and Manufacturing, 2001, 32,pp.1339-1343.
14. Gara F, Ranzi G, Leoni G. Simplified method of analysis accounting for shear-lag effects in composite bridge decks. Journal of Constructional Steel Research, 2011, 67,pp.1684-1697.
15. De Corte W, Delesie C, Van Bogaert P. Examination of local stresses in relation to fatigue failure at the rib to floorbeam joint of orthotropic plated bridge decks. Bridge Structures, 2007, 3,pp.183-191.
16. Konda N, Nishio M, Ichimiya M, et al. Development of fatigue test method and improvement of fatigue life by new functional steel plates for welding of trough rib and deck plate of orthotropic decks. International Journal of Steel Structures, 2013, 13,pp.191-197.

Research on Roller Circumferential Contour Model of Deformation Zone for Warm Rolling Strip

Li Zhijie, Wang Sufen, Zhou Zhaozhong

College of Mechanical Engineering, Quzhou University, Quzhou Zhejiang 324000, China

Corresponding author is Wang Sufen

Abstract
Study the circumferential contour of the deformation zone in the strip warm rolling, according the flow stress characteristic of warm deformation, the contact arc of deformation area is divided into three different curvature arc, the roller elastic flattening model of deformation zone is established using the method of quadratic curve fitting. The roller circumferential contour was calculated that iterative solver the roller elastic flattening deformation area and the distribution of rolling force along the rolling direction. Deformation process of warm-rolling was simulated using ANSYS/LS-DYNA finite element, the trend with simulation and calculated in the forward and backward slip zone is accordance, the model is more consistent with deformation process of the strip warm rolling.
Key words**:** WARM ROLLING, UNIT ROLLING PRESSURE, QUADRATIC CURVE FITTING, CIRCUMFERENTIAL CONTOUR